Insights into the enhanced oxidation of organic micropollutants by single-atom Cu catalyst activated peroxydisulfate: Valence-dominated nonradical pathway

Jingwen Pan [a,b], Xinyuan Wang [a], Xinyu Yang [a], Congcong Guo [a], Qinyan Yue [b], Xing Xu [b], Lei Wang [a], Yue Gao [b,*], Baoyu Gao [b]

[a] College of Environment and Safety Engineering, Qingdao University of Science and Technology, Qingdao 266042, PR China
[b] Shandong Key Laboratory of Water Pollution Control and Resource Reuse, School of Environmental Science and Engineering, Shandong University, Qingdao 266237, PR China

ARTICLE INFO

ABSTRACT

Herein, we anchored Cu atoms with four N atoms into waste adsorbent-based biochar (SACu$_{30}$@NC) containing both Cu(I) and Cu(II) to explore the role of different Cu valences for PDS activation mechanism. The atomic Cu was identified as the active site, and Cu(III) and electron shuttle process dominated organics degradation in SACu$_{30}$@NC/PDS system. Therein, Cu(I) preferred to activate the adsorbed PDS to produce Cu(III) (Cu(I)N$_4$-PDS→Cu(II)N$_4$-SO$_4^{\bullet-}$→Cu(III)N$_4$-SO$_4^{2-}$), whereas PDS adsorbed on Cu(II) surface was more likely to extract electrons from organic pollutants directly. Benefiting from non-radical process, SACu$_{30}$@NC exhibited selective and anti-interference performance for organic pollutants in complex matrixes. The promising catalytic activity of SACu$_{30}$@NC (BPA=50 mg/L, 100% within 180 min) with low Cu leaching (<0.1 mg/L) in continuous-flow experiments further revealed the potential of SACu$_{30}$@NC for practical applications. This work provides new insights into the PDS activation mechanism by single-atom Cu catalysts and develops an efficient approach for practical wastewater purification.

1. Introduction

Sulfate radical-based advanced oxidation processes (SR-AOPs) through the activation of persulfate (PS, including peroxymonosulfate (PMS) and peroxodisulfate (PDS)) has attracted ongoing attentions, which are the potential alternative to the classic Fenton system[1]. Nonradical oxidation pathways occurred in heterogeneous catalysis systems (catalyst/PS) have been confirmed to selectively attack electron-rich organics and tolerate complex water matrices, and reduce the generation of some highly toxic intermediates, compared to the conventional radical oxidation pathway[2,3]. Singlet oxygen ($^1O_2$) is the prevalent nonradical species with relatively mild oxidizing ability and high selectivity for pollutant degradation, which reacts with unsaturated organics via electron abstraction and electrophilic addition [4]. However, short-lived $^1O_2$ has slow reaction kinetics and consumes additional PS during pollutants degradation, which is limited in practical applications[5].

Alternatively, mediated electron transfer and high-valent metals have been proven as effective nonradical oxidation pathways[6,7]. For the electron transfer pathway, the reactive catalyst-PS complex is formed after PS adsorption onto catalysts, and organics degradation combined with PS decomposition occurs when pollutants donate electrons to the catalyst-PS complex[8]. However, it is unclear whether organics attacked by the catalyst-PS complex directly (adjacent transfer) or transfer electrons to catalyst-PS complex via catalysts (electron shuttle), so understanding these two processes is significant. In typical high-valent metal mechanisms, high-valent metal species, such as Fe (IV)/Fe(V), Co(IV), and Cu(III), are produced through the activation of stable-valent metal species by PS[9]. Organics are directly oxidized with little scavenging effect in high-valent metal species dominated systems, resulting in a higher PS utilization efficiency than other activation pathways[10–12]. Different from Fe(IV)/Fe(V) and cobalt (IV), the Cu (III) species is a highly oxidizing, low-toxicity species that promotes pollutant degradation through more abundant pathways[13–15]. Cu (III) was confirmed to be the main intermediate oxidant in homogeneous Cu(II)/PMS and Cu(II)/PDS systems[13,16]. However, homogeneous Cu

* Corresponding author.
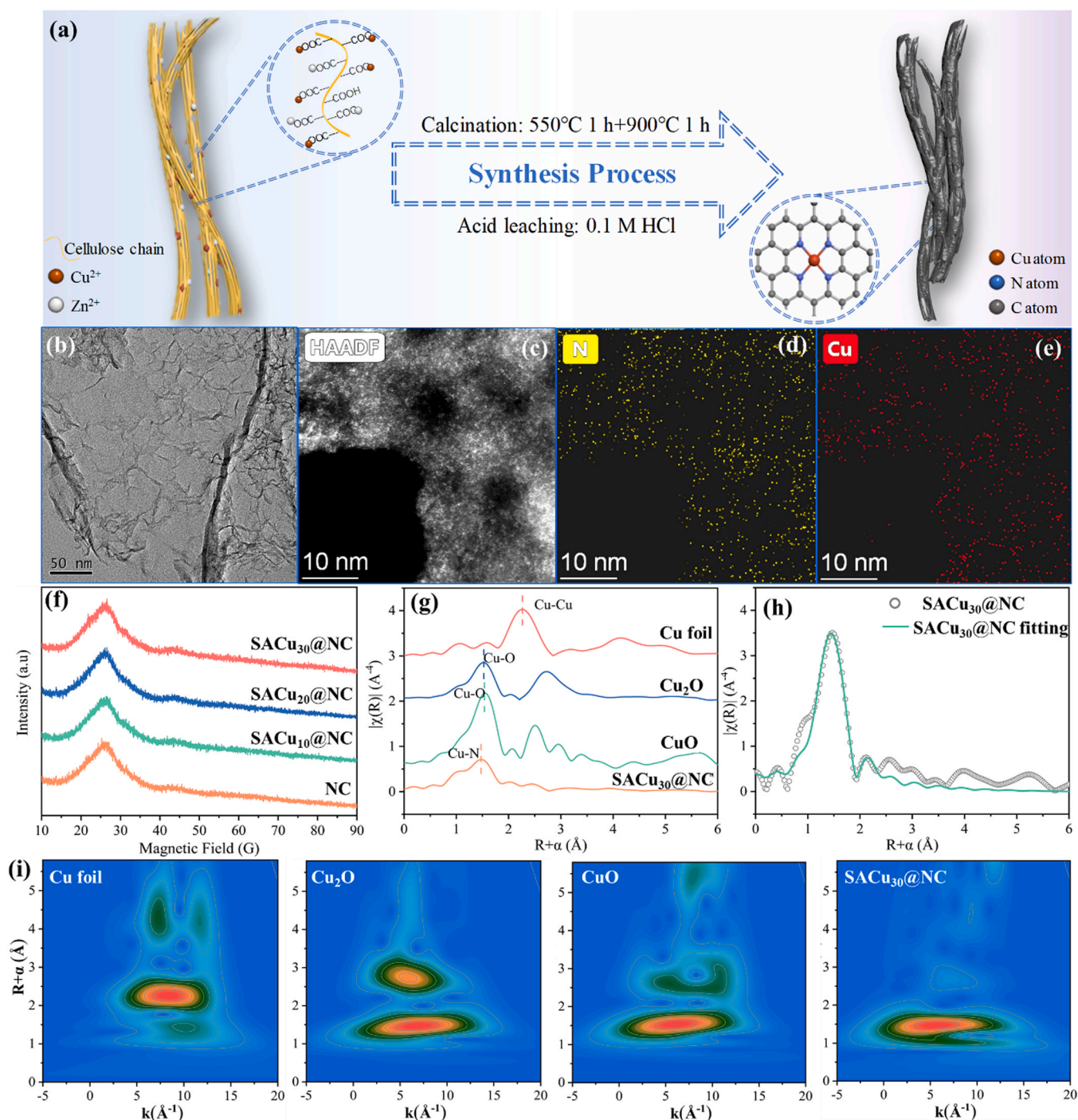 E-mail address: ygao@sdu.edu.cn (Y. Gao).

Fig. 1. (a) Fabricating scheme of SACu$_{30}$@NC using waste biosorbent as starting material; (b) HRTEM, (c) HADDF-HRTEM and (e) HRTEM mapping of SACu$_{30}$@NC; (f) XRD patterns of SACu$_x$@NC; (g) FT-EXAFS spectra of SACu$_{30}$@NC; (h) EXAFS R-space fitting curve of SACu$_{30}$@NC; (i) WT-EXAFS spectra of different samples.

(III) can only be produced under the alkaline or neutral conditions with Cu(II) mainly presenting as Cu(OH)$_2$ precipitate[16]. Lately, heterogeneous Cu(III) has been detected in PS catalytic activation by different nano Cu-based catalysts[17–19]. Note that the reduction potential of Cu (III) to Cu(II) in the ionic state is 1.57 V, but it would increase to 2.3 V in the heterogeneous catalysis[19,20]. However, solid-phase copper-based catalysts not only reduced copper utilization but also hindered the identification of active sites and related activation mechanisms. It is necessary to construct heterogeneous Cu-based catalysts with more uniform Cu to identify the role of active sites persulfate activation.

Single-atom catalysts (SACs) with isolated atomic metals, well-defined active sites, and controllable local structures may provide an appropriate opportunity to reveal the relationship between activity and catalysis mechanism. Recently, Li et al. anchored a single Cu atom with two pyridinic N atoms for PS activation to decompose 2, 4-dichlorophenol, and the unsaturated CuN$_2$ structure with Cu(II) promoted the formation of Cu(III)[21]. Chen et al. synthesized single-atom Cu-based catalysts with Cu(I)/Cu(II) in CuN$_4$ and Cu$_2$N$_6$ configurations to activate PS, the organics were decomposed by the electron transfer mechanism [22]. Hence, metal valence and configuration in SACs play an important role in PS activation for pollutants degradation. Bakandritsos et al. demonstrated that Cu(I) and Cu(II) played different roles in O$_2$-mediated
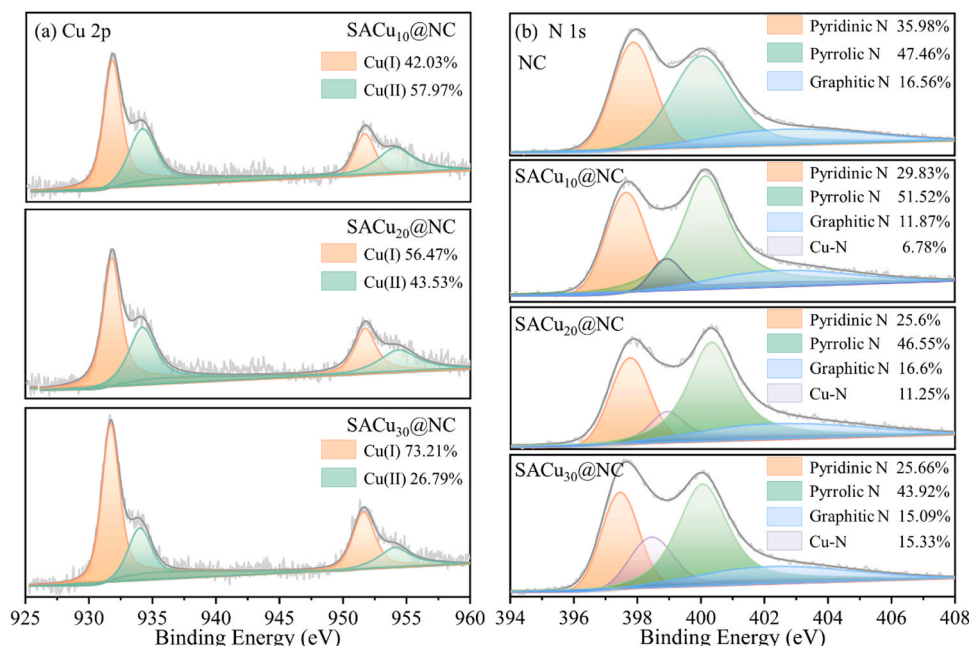
Fig. 2. (a) Cu 2p and (b) N 1 s XPS spectra of different SACu$_x$@NC sample.

oxidative coupling of amines and benzylic C-H bonds oxidation, though their synergistic effects cannot be overlooked[23]. Therefore, we reasonably speculate that the same phenomenon should also occur in the PS-mediated advanced oxidation, and exploring the effect of single-atom metal valence states on PS activation would provide new insights into the catalytic mechanism. Copper atoms in single-atom Cu catalysts mostly exist as the saturated CuN$_4$ configuration[24–26], which is more representative, and using it as a model to deeply study the effect of the atomic Cu valence state on the Cu(III) and other mechanisms in PS activation process is the most fundamental.

To solve the above issues, a single-atom Cu catalyst (SACu$_{30}$@NC) with saturated CuN$_4$ sites with two valences was designed in this study for efficient PDS activation for organic micropollutants degradation. The main objectives of this study were to (i) explore the effect of different valence states of copper atoms in SACu$_{30}$@NC on the PDS activation mechanism; (ii) distinguish the pathways of electron transfer processes in the SACu$_{30}$@NC/PDS system; (iii) reveal the evolution of the CuN$_4$ site during the PDS activation process for bisphenol A (BPA) degradation. This work advanced mechanism understandings of heterogeneous single-atom Cu catalysts associated with persulfate activation and would inspire subsequent research to explore the Fenton-like catalysis in-depth from the atoms valence state of single-atom catalysts.

2. Experimental section

2.1. Materials and methods

Details of materials and regents are listed in Text S1. The relevant details of characterization, experimental procedure, electrochemical analysis and theoretical calculations are given in Test S6.

2.2. Synthesis of SACu$_{30}$@NC

Typically, the SACu$_{30}$@NC activator was synthesized by simple pyrolysis. The spent biosorbent with adsorbed Cu^{2+} and Zn^{2+} ions (28.2 mg/g and 30.8 mg/g, respectively) was mixed and ground with 10 times weight of dicyandiamide and placed into a tube furnace. Above mixture was calcined at 550 °C for 1 h and then at 900 °C for another 1 h under N$_2$ protection (heating rate of 10 °C/min). After cooling, the SACu$_{30}$@NC was washed with HCl, deionized water and EtOH, and

dried at 60 °C for use. The catalysts obtained with different amounts of adsorbed Cu^{2+} (0, 11.3, 22.7 and 28.2 mg/g) were named as NC, SACu$_{10}$@NC, SACu$_{20}$@NC and SACu$_{30}$@NC, respectively.

2.3. Analytical methods

The concentration of organics was analyzed by a high-performance liquid chromatograph (waters 1515, U.S.A) equipped with a C18 column and UV–vis detector. The analytical method details of different organics are provided in Table S1. The residual PDS concentration was detected by a chromogenic method using N, N-Diethyl-p-phenylenediamine sulfate (NDPDAS) as the chromogenic agent. Typically, 0.2 mL sample was added to a mixing solution (0.4 mL of 100 mM NDPDAS, 8.4 mL acid deionized water and 1 mL of 40 mM FeSO$_4$,) and shaken promptly, which was measured at λ=510 nm on a UV–vis spectrophotometer after 1.5 min of color rendering. Cu(III) was determined by complexing with periodate to form a stable Cu(III)-periodate complex and detected at 415 nm.

3. Results and discussions

3.1. Synthesis and characterization of SACu$_{30}$@NC

SACu$_{30}$@NC with atomically dispersed Cu was prepared by in-situ calcination using biosorbents saturated with copper and zinc ions (Fig. 1a). HRTEM image (Fig. 1b) displays that SACu$_{30}$@NC consists of flat two-dimensional carbon layers without any nano-metal particles. In Fig. S1, BET specific surface area of SACu$_{30}$@NC reached 182.80 m^2/g higher than that of NC (155.37 m^2/g), implying that introduced Cu promoted specific surface generation, providing more active sites and facilitated the mass transfer of pollutants and PDS[27]. The larger specific surface area of SACu$_{30}$@NC could be ascribed to the existence of Cu atoms promoting the exfoliation of NC[26]. HADDA-HRTEM was performed to further visualize the dispersion of atomically-dispersed Cu sites (Fig. 1c-e). Numerous isolated light spots were observed in saturated biosorbent-based carbon matrixes (Fig. 1c). EDS element mappings of SACu$_{30}$@NC exhibited that both N and Cu species were well dispersed with no Cu nanoparticles present (Fig. 1d-e). XRD patterns of different SACu$_x$@NC catalysts displayed similar peaks compared to NC catalysts without the specific peak of Cu nanoparticles (Fig. 1f). Above
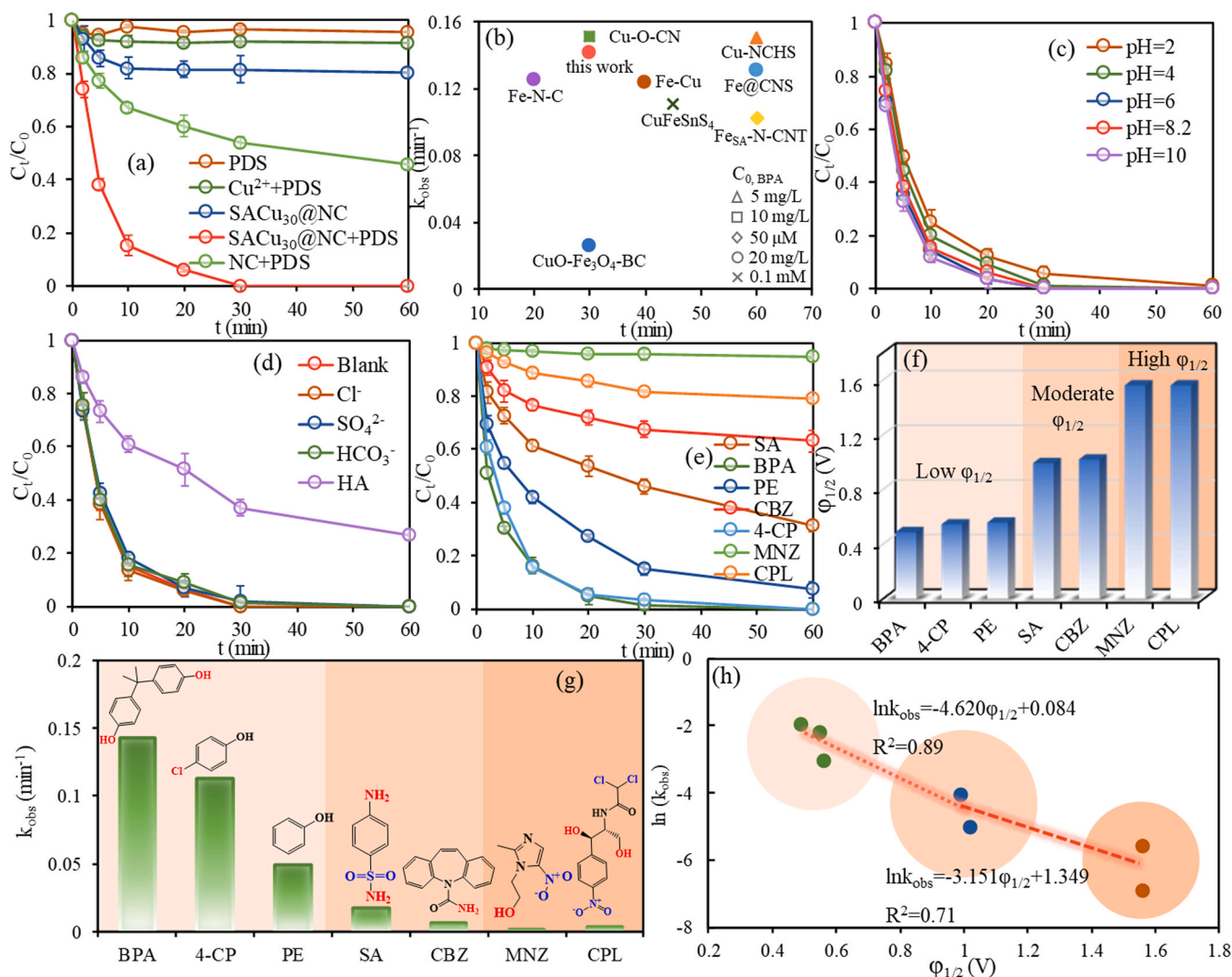
Fig. 3. (a) BPA degradation in different systems; (d) comparison of BPA degradation in various PDS activation systems; effect of (c) pH and (d) anion and humic acid on BPA degradation; (e) Oxidation, (f) $\varphi_{1/2}$ values and (g) k_{obs} values of different pollutants in SACu$_{30}$@NC/PDS system; (h) Relationship between $\varphi_{1/2}$ values of different pollutants and their k_{obs}. (Reaction conditions: catalyst dosage=0.1 g/L, [PDS]$_0$=0.2 g/L, [BPA]$_0$=20 mg/L, [Cl$^-$]$_0$=[SO$_4^{2-}$]$_0$=[HCO$_3^-$]$_0$=50 mg/L (if any), [HA]$_0$=10 mg/L (if any), [BPA]$_0$=[SA]$_0$=[PE]$_0$=[CBZ]$_0$=[4-CP]$_0$=[MNZ]$_0$=[CPL]$_0$=0.1 mM, T=25℃).

results implied that the atomically-dispersed Cu sites had been successfully anchored onto the carbon layers.

The coordination environment of Cu atoms in SACu$_{30}$@NC was further confirmed by XAS analysis. The XANES spectra indicated that the absorption near the edge of atomically-dispersed Cu sites in SACu$_{30}$@NC was close to the Cu$_2$O and its line edge was located between the Cu$_2$O and CuO (Fig. S2), indicating that the Cu atoms were coordinated in Cu(I) and Cu(II) forms in SACu$_{30}$@NC. The FT-EXAFS spectrum of SACu$_{30}$@NC showed a peak at 1.44 Å (Fig. 1g) assigned to the backscattering of Cu-N coordination[28]. Additionally, no typical Cu-Cu (2.27 Å) and Cu-O (1.56/1.47 Å) coordination peaks appeared, which suggested that Cu atoms were isolated from each other and conjoined to N atoms in SACu$_{30}$@NC. The corresponding WT-EXAFS results further verified that Cu-Cu and Cu-O bonds did not exist in SACu$_{30}$@NC (Fig. 1i), and that only a maximum k value at 5.2 A^{-1} was observed, which corresponded to Cu-N[29]. Furthermore, the quantitative coordination configuration of iron sites in SACu$_{30}$@NC was deduced to be 4.35±0.4, which was similar to that of CuPc and distinct from Cu foil, CuO, and Cu$_2$O (Fig. 1h and Table S2) and the average bond length of Cu-N was approximately 1.92 Å.

XPS analysis was applied to identify the surface elements of the catalysts (Fig. 2a, and Fig. S3). The peaks at ~931.8/951.6 eV and ~

934.1/954.6 eV indicated the Cu(I) and Cu(II) existed in different SACu$_x$@NC catalysts, respectively (Fig. 2a)[30]. Cu(I) content gradually increased with the increasing Cu atoms loading, while the Cu(II) content gradually decreased. And copper oxidation or Cu^0 were not observed in SACu$_x$@NC, proving the successfully fabrication of the Cu single-atoms embedded into biochar. New peaks (N-Cu) appeared in N 1 s XPS spectra near 398.9 eV when introducing Cu atoms into carbon matrixes and increased with the rising Cu atoms content (Fig. 2b), which also suggested that Cu atoms coordinated with N atoms. Meanwhile, N1s XPS spectra of the SACu$_x$@NC catalysts showed a small shift (0.1–0.42 eV) and a notable decrease in content of pyridine N in both SACu$_{10}$@NC, SACu$_{20}$@NC and SACu$_{30}$@NC as compared with that of NC. As result, the Cu single-atoms were coordinated with pyridine N to form the Cu-N$_4$ configurations.

3.2. Catalytic performance of SACu$_{30}$@NC with PDS activation

The catalytic performance of SACu$_{30}$@NC was evaluated by BPA degradation with PDS activation. BPA cannot be decomposed by PDS alone (Fig. 3a), approximately 20% BPA could be rapidly adsorbed onto SACu$_{30}$@NC surface. With the activation of PDS, BPA can be completely removed within 30 min in SACu$_{30}$@NC/PDS system, whereas only 9% of
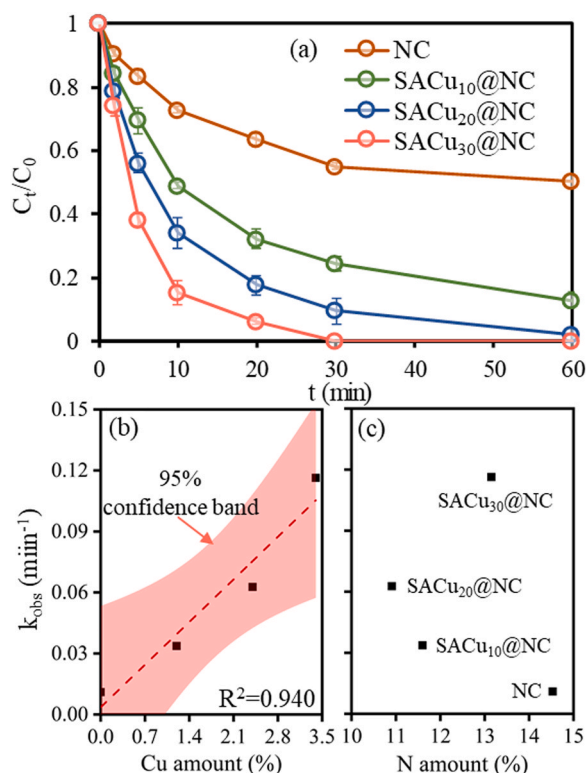
Fig. 4. (a) The degradation curves of BPA in different SACu$_x$@NC system (catalyst dosage=0.1 g/L, [PDS]$_0$=0.2 g/L, [BPA]$_0$=20 mg/L, T=25℃); the correlation between BPA removal rate and (b) Cu (%) content and (c) N (%) content.

BPA was degraded in Cu^{2+}/PDS system, indicating that the Cu^{2+} possibly dissolved from catalyst cannot effectively activate PDS for BPA degradation. Meanwhile, SACu$_{30}$@NC/PDS system could effectively remove TOC and reach 71.1% mineralisation rate at 60 min (Fig. S4). The significantly enhanced degradation rate of SACu$_{30}$@NC compared with NC implied that the introduced atomic Cu provided additional active sites into the carbon layer. Comparison of k_{obs} for BPA degradation with other reported Cu-based and single atom catalyst/PS systems are given in Fig. 3b and Table S3 [7,31–37]. Results confirmed the ultrahigh catalytic activity of SACu$_{30}$@NC for heterogeneous PDS activation and showcased the excellent catalytic activity of single-atom Cu active sites. BPA degradation at different pH values in Fig. 3c shows a steady upward trend as the pH increased from 2.0 to 10 with k_{obs} in the range of 0.080–0.171 min^{-1}. And ~0.08 mg/L of Cu^{2+} ions were released from the SACu$_{30}$@NC catalyst at pH=2, and it was decreased to below 0.02 mg/L under neutral and alkaline environments (Fig. S5). These results also indicated that the Cu^{2+} ions released from SACu$_{30}$@NC did not contribute to BPA removal. BPA degradation in SACu$_{30}$@NC/PDS system with the background of humic acid (HA) and different anions showed that 100% BPA degradation still could be reached with the interference of anions (Fig. 3d). However, a noticeable reduction of BPA degradation efficiency was inevitable in HA solution, which might due to that active sites on the surface of SACu$_{30}$@NC were occupied by HA.

Different organic pollutants were degraded in SACu$_{30}$@NC/PDS system and different organics showcased different degradation rates (Fig. 3e and g). BPA and 4-chlorophenol (4-CP) could be completely oxidized and 93% phenol (PE) was removed within 30 min. Contrastively, carbamazepine (CBZ), sulfanilamide (SA) metronidazole (MNZ), and chloramphenicol (CPL) were only partially degraded with relatively low rates of oxidation, especially MNZ (<0.001 min^{-1}). The above results suggested the oxidation selectivity of different organic pollutants in

SACu$_{30}$@NC/PDS system. The different removal trends might be due to the versatile oxidation origins of the targeted organic pollutants. The half-wave potential ($\varphi_{1/2}$) of different organics could represent the redox potential of the pollutants (Fig. 3f, Table S4)[38], and these organics could be classified into three categories. BPA showed the lowest $\varphi_{1/2}$ value among all selected organics, and it was followed by 4-CP< PE< SA< CBZ< MNZ< CPL. The relationship between the $\varphi_{1/2}$ values of different organics and their k_{obs} values obtained in SACu$_{30}$@NC/PDS system is shown in Fig. 3h. The $\varphi_{1/2}$ values (lower than 1.1 V) of five pollutants (BPA, CP, PE, SA and CBZ) exhibited significant correlations with their ln$_{kobs}$. In contrast, MNZ and CPL showed very low ln$_{kobs}$ values, which were deviated from the correlated lines. These results indicated that the SACu$_{30}$@NC/PDS system had a well-selective oxidative capacity for pollutants correlated with the redox potential of the pollutants.

3.3. Activities of SACu$_x$@NC and role of atomic Cu

Adsorption and catalytic performance of different activator with different amounts of Cu anchored are displayed in Fig. 4a and Fig. S6. The as-prepared activators had a weak adsorption capacity (~20%) towards BPA. Contrastively, both SACu$_{30}$@NC/PDS and SACu$_{20}$@NC/PDS systems showed fast oxidation activity with 100% of BPA decomposition within 60 min. And the SACu$_{30}$@NC exhibited a higher activation activity towards PDS than that of SACu$_{20}$@NC, which showed 0.86-fold enhancement in the BPA degradation. As Cu atom content decreased continuously, BPA cannot be completely degraded in a catalytic system, and only 50% BPA was removed when the catalyst was free of anchored Cu atoms. This result indicated that the introduction of Cu atoms could effectively improve the reactivity of the catalyst. To explore the intrinsic influencing factors on BPA degradation and distinguish the role of the introduced Cu and N in catalysts, the correlation between BPA degradation rate and Cu/N content in different systems was analyzed. The degradation rates of BPA showed a well-positive correlation (R^2=0.940) with the content of loaded Cu (%, Fig. 4b), that was, the more Cu atoms, the higher reaction rate. This also proved that anchored Cu atoms might be the main factor for the catalyst performance. Conversely, the N content (%) had no linear correlation with BPA degradation performance (Fig. 4c), implying that the inducted N in SACu$_x$@NC did not directly affect their catalytic capacity.

3.4. Insight into the catalyst mechanism

3.4.1. Identification of reactive oxygen species

To discern the underlying reasons that contributed to the improved catalyst performance after the Cu atoms introduction, we examined the PDS activation pathway in SACu$_{30}$@NC/PDS system. As shown in Fig. 5a, excess amounts of EtOH and TBA used as scavengers of SO$_4^{\bullet-}$ and •OH had a negligible impact on BPA degradation, implying that SO$_4^{\bullet-}$ and •OH were not the main active species in SACu$_{30}$@NC/PDS system. Nevertheless, significant signals belonging to the DMPO-SO$_4^{\bullet-}$ and DMPO-•OH adducts were observed in SACu$_{30}$@NC/PDS/BPA system (Fig. 5d)[39], which indicated that SO$_4^{\bullet-}$ and •OH were generated during PDS activation process. The intensity of DMPO-SO$_4^{\bullet-}$ and DMPO-•OH adducts decreased gradually with the decline of Cu atom content. The results suggested that the introduced Cu atoms could promote the generation of SO$_4^{\bullet-}$ and •OH, however, this was not consistent with the quenching results. This was probably due to that the generated free radicals were ineffective for the degradation of BPA, which will be further explained in the following.

FFA was used as the scavenger for ^{1}O$_2$[40], which inhibited the BPA degradation apparently (Fig. 5a), suggesting a potential contribution of ^{1}O$_2$ in SACu$_{30}$@NC/PDS system. However, during BPA degradation, FFA competed with BPA to deplete the produced active species, leading to a decrease in BPA degradation efficiency[41].The characteristic signal of DMPO-^{1}O$_2$ adducts was not observed in the TEMP-trapping
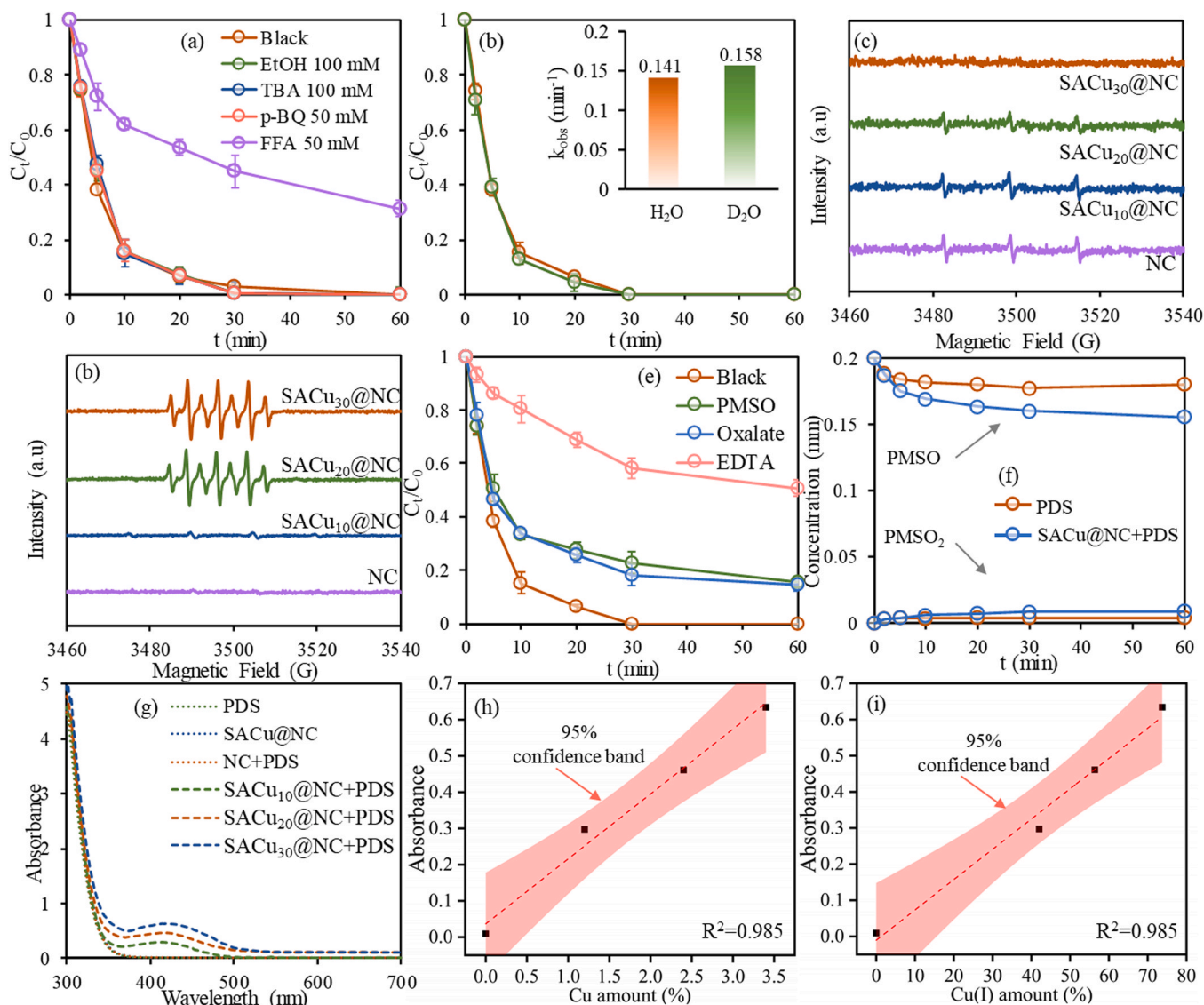
Fig. 5. Effect of (a) scavenger and (b) D_2O on BPA degradation in SACu$_{30}$@NC/PDS system; (c) EPR spectra of $^1O_2$ and SO$_4^{•-}$/•OH in different SACu$_x$@NC/PDS/BPA system; (e) Effect of PMSO, oxalate and EDTA on BPA degradation kinetics; (f) PMSO and PMSO$_2$ concentrations in PDS alone and SACu$_{30}$@NC/PDS systems; (g) detection of Cu(III) by the periodate colorimetric method in the different system; influence of (h) Cu atoms amount and (i) Cu(I) amount on the absorbance at 415 nm. (catalyst dosage=0.1 g/L, [PDS]$_0$=0.2 g/L, T=25℃, [BPA]$_0$=20 mg/L, [PMSO]$_0$=[Oxalate]$_0$=[EDTA]$_0$=0.2 mM (if any)).

EPR spectra (Fig. 5c), differing from the FFA quenching result. To further confirm the role of $^1O_2$ in SACu$_{30}$@NC/PDS system, BPA degradation was performed in D_2O, due to that the life time of $^1O_2$ in D_2O (20–30 μs) was longer than that in H_2O[3]. In the SACu$_{30}$@NC/PDS system after replacing H_2O with D_2O as the solvent, the degradation rate of BPA was only enhanced by 12% (Fig. 5b), suggesting that $^1O_2$ is not the main active species for BPA degradation in this system. Therefore, other nonradical mechanisms were present in the SACu$_{30}$@NC/PDS system.

3.4.2. Identification of Cu(III) species and electron-transfer process

High-valent copper species have been reported as the dominant PDS activation mechanism in some Cu-based SR-AOPs[42]. The mechanism was confirmed as PDS bound with Cu(II) sites to generate Cu(III)-O, which could efficiently eliminate organics[18,19]. While the process of reaction of PDS with Cu(II) sites to generate Cu(III) has not been clarified. To identify the possible Cu(III) species in SACu$_{30}$@NC/PDS system, oxalate and EDTA were used to impede the formation of Cu(III). When the Cu atom sites were chelated with carboxyl groups of oxalate

and EDTA, the formation of Cu(III) species was inhibited, further hindering organics removal[43]. As shown in Fig. 5e, BPA removal was slightly inhibited after adding oxalate in SACu$_{30}$@NC/PDS system, while it was severely inhibited by the addition of EDTA. This indicated Cu(III) may be involved in SACu$_{30}$@NC/PDS system. PMSO as the chemical probe could be oxidized to PMSO$_2$ by high-valent metal-oxo intermediates[44]. The BPA removal was inhibited as 0.2 mM of PMSO was added (Fig. 5e), indicating the possible presence of Cu(III). Furthermore, the PMSO consumption and PMSO$_2$ generation were also detected to conform to the Cu(III). Approximately 10% of PMSO was consumed when PDS alone (0.2 g/L) was used, while its consumption was elevated to 20% in the SACu$_{30}$@NC/PDS system, however, the PMSO$_2$ production was not significantly elevated when SACu$_{30}$@NC was mixed with PDS (Fig. 5f). Since PDS can also react with PMSO to form PMSO$_2$, but with a slower oxidation rate, these results suggested that Cu(III) formed by SACu$_{30}$@NC was not ligated with O to participate in the generation of PMSO$_2$.

To further verify that Cu(III) was the main working oxidant in SACu$_{30}$@NC/PDS system, other solid evidence was also provided. Cu
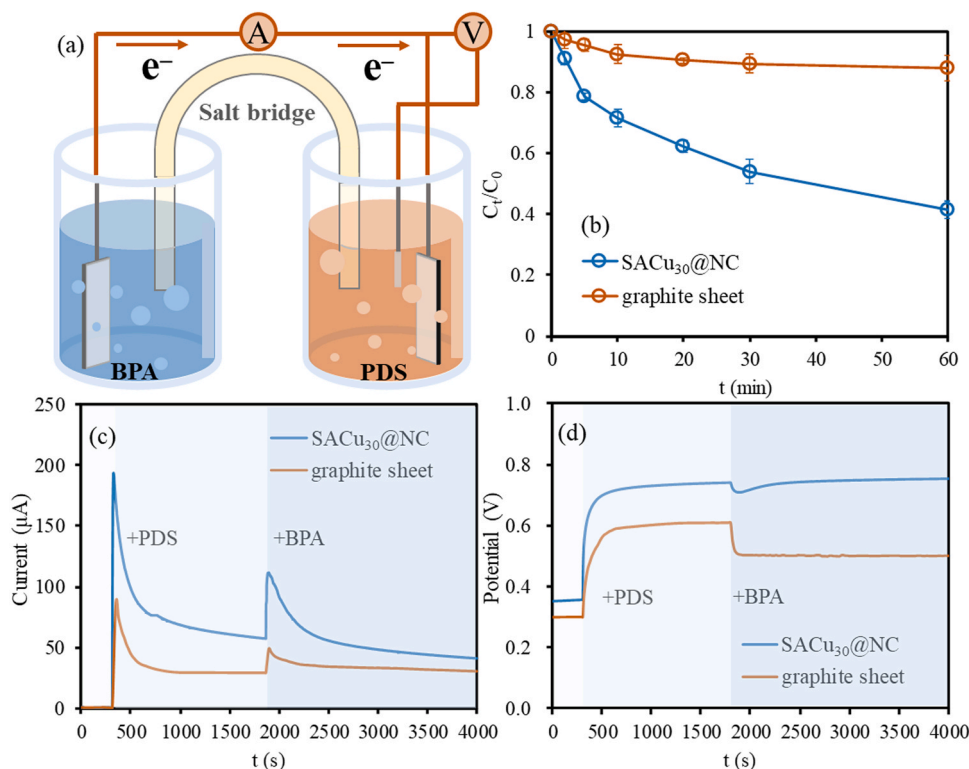
Fig. 6. (a) scheme of GOS device; (b) BPA degradation in different GOS; (c) the current and (d) in-situ electric potential of anode (vs Ag/AgCl) in GOS.

(III) was not stable, but periodate was able to stabilize Cu(III) by forming Cu(III)-periodate complex, which was equipped with a characteristic absorbance at 415 nm[16]. Interestingly, significant absorbance at 415 nm was observed when periodate was added into SACu$_{30}$@NC/PDS system, while no absorbance was found for SACu$_{30}$@NC and PDS alone (Fig. 5g). Moreover, the absorbance diminished with decreasing Cu atom content, and characteristic peak of Cu(III)-periodate complex disappeared in NC/PDS system. The correlation between Cu (III)-periodate complex and Cu atom content was also explored (Fig. 5h). The results showed that the absorbance intensity of Cu (III)-periodate complex increased linearly with increased Cu content. XAS and XPS analyses showed the presence of two valence states (Cu(I) and Cu(II)) of Cu atoms in SACu$_{30}$@NC. The Cu(I) content also exhibited a high positive correlation with the absorbance of Cu(III)-periodate complex (Fig. 5i), suggesting that the formation of Cu(III) may be related to Cu(I). The absorbance intensity of Cu(III)-periodate complex decreased significantly after adding oxalic acid and EDTA into SACu$_{30}$@NC/PDS system (Fig. S7). These supported the above results that Cu(III) species, possibly derived from Cu(I), were present in the oxidation system, and further evidences would be provided later.

Although Cu(III) had been identified to play an essential role in SACu$_{30}$@NC/PDS system, it can still oxidize BPA in the presence of high concentrations of chelating agents, suggesting that other oxidation mechanisms existed in SACu$_{30}$@NC/PDS system. electron transfer process also has been proven to be an important mechanism for organics elimination in SR-AOPs[45,46]. The open-circuit potential was applied to validate the electron transfer process. At the beginning of the reaction without PDS, the potential of SACu$_{30}$@NC remained stable (Fig. S8), but increased immediately after the addition of PDS and gradually achieved a plateau. This process can be explained as PDS adsorbed on the surface of the catalyst to produce active complexes, and gradually reaching dynamic equilibrium. When the potential of the active complex exceeded the oxidation potential of the organics, the active complex would oxidize the organics through an electron transfer process[46]. Meanwhile, the equilibrium potential increased gradually with the growing

Cu atom content in the catalyst, which indicated that the electron transfer process was also initiated by the Cu atom sites. Besides, the impedance of the catalysts gradually reduced as the Cu atom content increased (Fig. S9), which also facilitated the electron transport in the catalytic oxidation process.

To further demonstrate the electron transfer mechanism, a galvanic-oxidation system (GOS) was designed which separated PDS and BPA into two tanks and used catalyst-coated graphite sheet (GS) as electrode to distinguish between electron adjacent transfer and electron shuttle processes (Fig. 6a). In the GOS, the current between the anode and cathode as well as the in-situ potential of the cathode were simultaneously detected to clarify the microscopic process of the reaction. As shown in Fig. 6b, the BPA was rapidly degraded by using SACu$_{30}$@NC-coated GS, which strongly supported the electron shuttle mechanism of the SACu$_{30}$@NC/PDS system. The electron shuttle between the anode and cathode tanks caused a surge of current (Fig. 6c). Meanwhile, decomposition of the PDS complex on SACu$_{30}$@NC-GS also resulted in a reduction of the cathodic potential (Fig. 6d). All these results strongly supported that electron shuttling was another dominant mechanism in SACu$_{30}$@NC/PDS system. A similar phenomenon was observed when uncoated GS were used, due to the ability of graphite to activate PDS via electron transfer process as well[47]. However, the GS electrode achieved a stronger decrease in cathodic potential than SACu$_{30}$@NC-GS after the addition of BPA to the anode tank. The active complex of PDS on GS failed to be replenished after rapid decomposition, while SACu$_{30}$@NC promoted the rapid production of the active complex. Taken together, Cu(III) species and the electron shuttle process were the main mechanisms for BPA degradation in SACu$_{30}$@NC/PDS system.

3.4.3. Mechanistic exploration based on DFT calculation

DFT calculations were further proceeded to probe the insights of PDS activation and BPA oxidization mechanism on the Cu atom sites. Based on the results of catalyst characterizations, two valence states of CuN$_4$ (Cu(I)N$_4$ and Cu(II)N$_4$) configurations were constructed (Fig. S10). The intermediate configurations and the corresponding energy status are
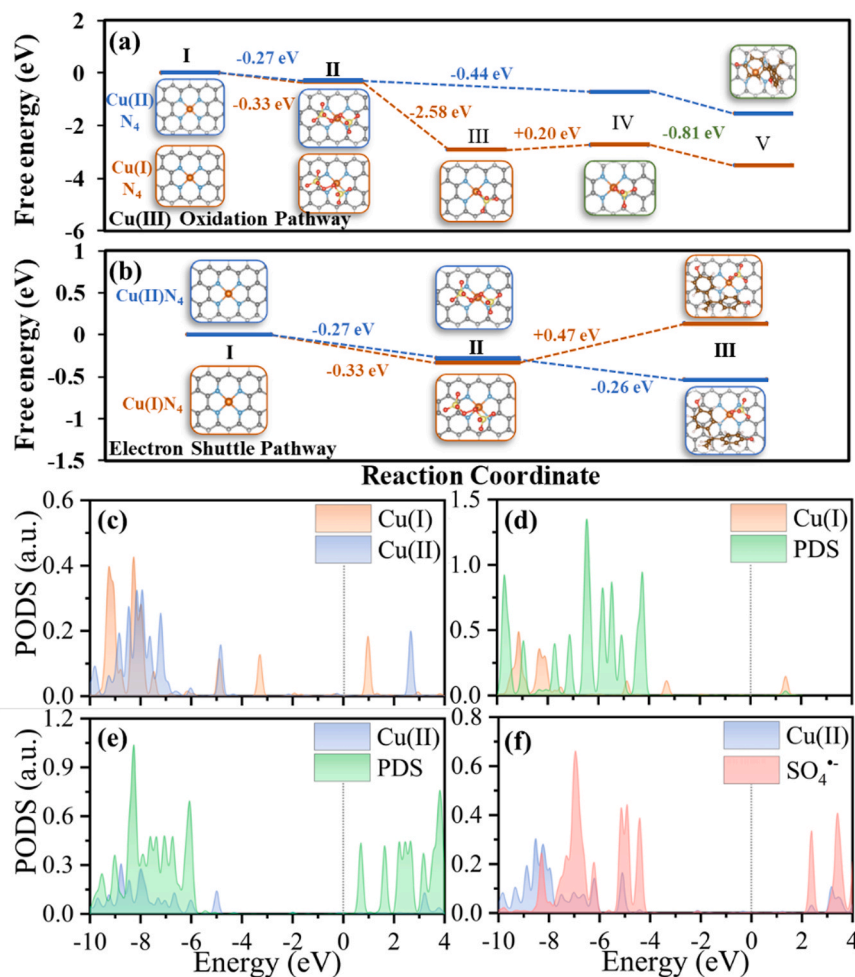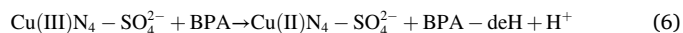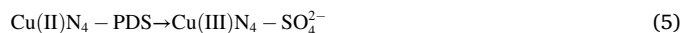
Fig. 7. Reaction pathways of PDS activation and BPA oxidation at Cu sites with different valences via (a) Cu(III) oxidation and (b) electron shuttle process (orange and blue routes represented reaction on Cu(I)N$_4$ and Cu(II)N$_4$ sites, and the green box represented the common structure); (c) PDOS of Cu atom in Cu(II)N$_4$ sites; (d) and (e) PDOS of PDS adsorbed on Cu(I)N$_4$ sites and Cu(II)N$_4$ sites; (f) PDOS of SO$_4^{\bullet-}$ adsorbed on Cu(II)N$_4$ sites.

shown in shown in Fig. 7, where the orange and blue routes represent the PDS activation and BPA degradation processes on Cu(I)N$_4$ and Cu(II)N$_4$. For the Cu(III)-dominated pathway (Fig. 7a), the CuN$_4$ adsorbed PDS (II) forming the Cu(I)N$_4$-PDS and Cu(II)N$_4$-PDS in the solution firstly and releases energy. Then, the adsorbed PDS was activated and Cu(I)N$_4$ was oxidized to Cu(II)N$_4$ present as Cu(II)N$_4$-SO$_4^{\bullet-}$ (III), which was converted to Cu(III)N$_4$-SO$_4^{2-}$ (IV), while the Cu(II)N$_4$ was oxidized to form the Cu(III)N$_4$-SO$_4^{2-}$ (IV). Subsequently, the pollutant BPA was attacked by Cu(III)N$_4$-SO$_4^{2-}$ and decomposed (V), and the corresponding process can be presented in Eqs. 1–6. The total energy released during the whole reaction on Cu(I)N$_4$ and Cu(II)N$_4$ was −3.52 and −1.52 eV, respectively, indicating that the formation of Cu(III) species and the oxidation BPA was thermodynamically favorable in the system of two valence copper atoms. Compared to Cu(II)N$_4$, the Cu(I)N$_4$ dramatically promoted the adsorption of PDS (I→II) and the formation of Cu(III) species (II→IV) at the CuN$_4$ site depending on the amount of released energy (Fig. 7a). This results implied that the Cu(I) form played a more important role in the Cu(III) oxidation mechanism.

$$Cu(I)N_4 + PDS \rightarrow Cu(I)N_4 - PDS \tag{1}$$

$$Cu(I)N_4 - PDS \rightarrow Cu(II)N_4 - SO_4^{\bullet-} \tag{2}$$

$$Cu(II)N_4 - SO_4^{\bullet-} \rightarrow Cu(III)N_4 - SO_4^{2-} \tag{3}$$

$$Cu(II)N_4 + PDS \rightarrow Cu(II)N_4 - PDS \tag{4}$$

$$Cu(II)N_4 - PDS \rightarrow Cu(III)N_4 - SO_4^{2-} \tag{5}$$

$$Cu(III)N_4 - SO_4^{2-} + BPA \rightarrow Cu(II)N_4 - SO_4^{2-} + BPA - deH + H^+ \tag{6}$$

For the electron shuttle process-dominated pathway (Fig. 7b), PDS was adsorbed onto the surface of Cu(II)N$_4$ sites (II), and CuN$_4$-PDS complex can directly oxidize the pollutants and PDS was reduced to sulfate ions (III) with the energy barrier calculated as −0.26 eV. This indicated that electrons of BPA were transferred directly to PDS for its own degradation, while Cu(II)N$_4$ sites acted as a transfer station. In contrast, Cu(I)N$_4$-PDS formed by Cu(I) adsorbed PDS required an additional 0.47 eV for BPA oxidation, which was energetically unfavorable, suggesting that the Cu(II) form performed a dominant role in the electron shuttle mechanism[48].

Partial density of states (PDOS) of Cu atom with different valances in intermediates I were calculated and shown in Fig. 7c. The 3d orbital electrons of Cu atoms in CuN$_4$ were mostly below the Fermi level, while the Cu(I) species electrons are closer to the Fermi energy level, suggesting that there was a stronger chemical reactivity between the Cu(I) species and PDS[49]. Subsequently, PDS was added and adsorbed on the surface of the CuN$_4$ sites to form intermediate II. As shown in Fig. 7d and e, the electron overlap of the Cu(II) 3d orbital with the PDS molecule was higher than that of Cu(I), indicating that Cu(II) reacted easily with PDS to form the PDS complex and the electrons was more easily transferred[50]. In contrast, PDS was decomposed on the surface of Cu(I) through strong chemical reaction to form intermediate III in the Cu(III)
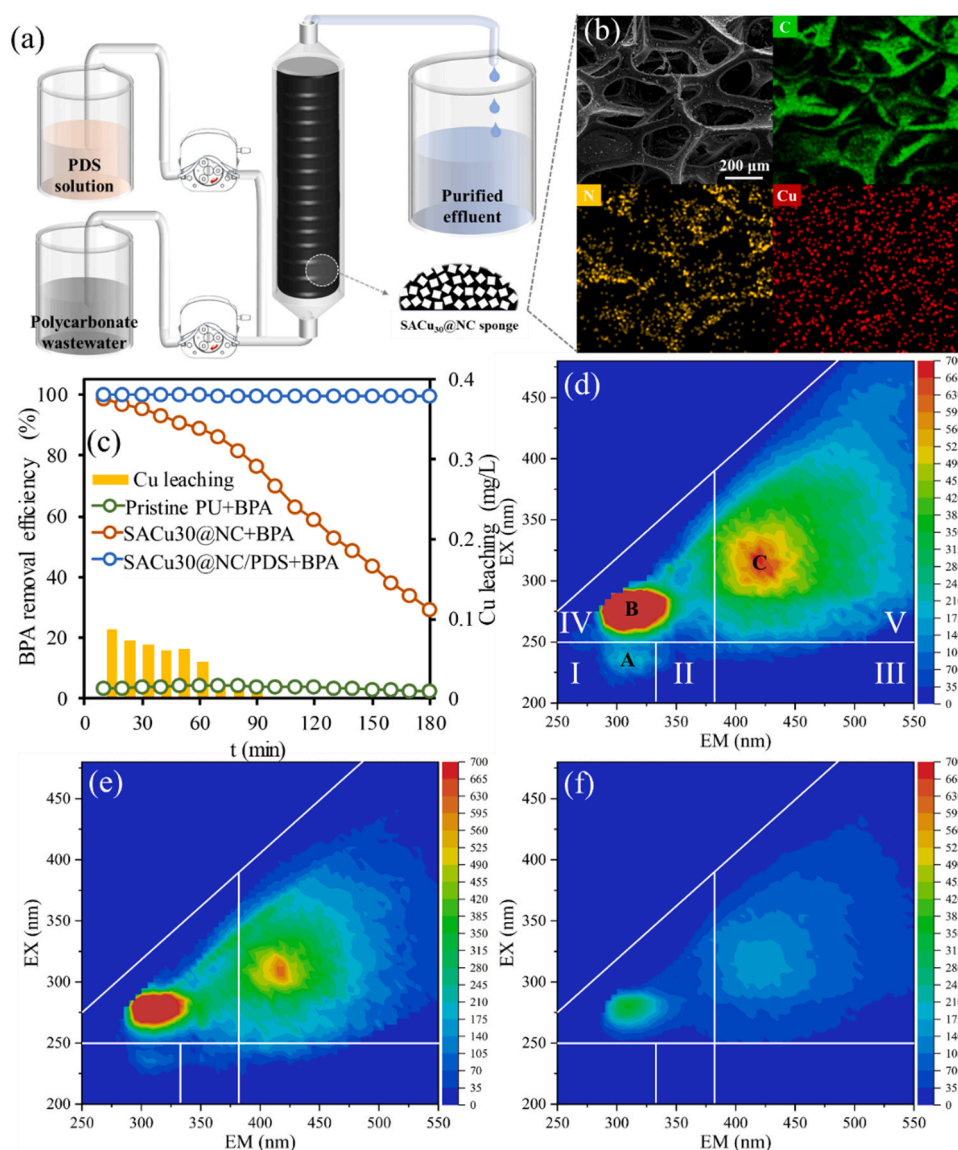
Fig. 8. (a) Schematic diagram of the dynamic degradation experiments; (b) SEM of the SACu$_{30}$@NC-loaded PU; (c) removal of BPA in the different system; (d) FEEM spectra obtained in PCW, effluents of (e) SACu$_{30}$@NC-loaded PU adsorption system, and (f) SACu$_{30}$@NC-loaded PU/PDS oxidation system.

oxidation pathway (Fig. 7f). Generated $SO_4^{\bullet-}$ was adsorbed on the surface of oxidized Cu(II), and the higher electron overlap implied that $SO_4^{\bullet-}$ was donated electrons easily from Cu(II) to produce Cu(III)-SO_4^{2-} (Eqs. 1–3) [7]. Based on the experimental results and DFT calculations, we reasonably propose that Cu atoms in CuN$_4$ were the main active site of SACu$_{30}$@NC, where the Cu(I) was mainly responsible for the formation of Cu(III) species, while the Cu(II) could either generate Cu(III) or form a complex with PDS to oxidize the pollutant directly through the electron shuttle process.

3.5. Continuous flow experiment

A microreactor (Fig. S11) filled with SACu$_{30}$@NC-loaded polyurethane (PU) sponges (prepared according to Text S7) was designed to simulate the real application of SACu$_{30}$@NC/PDS system. The PU was loaded with 100 mg of SACu$_{30}$@NC to form the catalytic filter and the mixture of wastewater and PDS was fed to the catalytic filter from bottom to top (Fig. 8a). SEM image of SACu$_{30}$@NC-loaded PU showed that the catalytic filter was composed of the higher density fibers (Fig. 8b). The EDS mappings indicated that the SACu$_{30}$@NC was well dispersed on the surface of the PU, thus forming large number active

sites for PDS activation. In SACu$_{30}$@NC-loaded PU/PDS system, BPA (50 mg/L) in polycarbonate wastewater (PCW, Table S5 and Fig. 8c) was completely oxidized in the catalytic filter for more than 3 h (flow rate: 2 mL/min). Contrastingly, the PU without coating SACu$_{30}$@NC and sole SACu$_{30}$@NC-loaded PU showed poor removal performance of BPA. These results suggested that SACu$_{30}$@NC-loaded PU/PDS was high-efficiency and could resist the interference of wastewater matrix in continuous operation. The Cu leaching during the long-time operation process was also detected. Approximately 80 µg/L of Cu was leached at first 10 min, and it was reduced to lower than 2 µg/L gradually with further processing, which indicated the stability of SACu$_{30}$@NC in the catalytic filter.

To further confirm the contribution of SACu$_{30}$@NBC-loaded PU (adsorption) and SACu$_{30}$@NBC-loaded PU/PDS (oxidation) system on the organics removal from PCW, the fluorescence excitation-emission matrix (FEEM) spectra of different effluent from the different systems were evaluated. As shown in Fig. 8d, fluorescence peaks in untreated PCW were centered approximately at the $\lambda_{EX/EM}=245/315$ nm (A), 275/315 nm (B), and 320/420 nm (C), which represented tyrosine, tyrosine-protein-like and humic acid-like contaminants, respectively[51,52]. The peaks A and B showed much weaker signals after adsorption (Fig. 8e and

Fig. S12), suggesting that some tyrosine and humic acid-like substances could be adsorbed onto the SACu$_{30}$@NBC-loaded PU. SACu$_{30}$@NBC captured organics mainly via physical adsorption and electrostatic attraction, so the large and electrically tyrosine-protein-like substances could not be effectively removed. In the catalytic-oxidation system, fluorescence intensity in all five regions reduced dramatically (Fig. 8f). Compared to the adsorption process, peaks B and C in the oxidation system decreased significantly and peak A disappeared completely, implying that the Cu(III) and electron shuttle dominated oxidation pathways can effectively change or destroy the structure of organic pollutants, even the refractory humic acid-like organics.

4. Conclusion

This work synthesized Cu single-atom catalysts with Cu(I) and Cu(II) valence states using waste biosorbent as carbon supports to clarify the effect of metal valence states on the PDS activation mechanism. Cu(III) derived from saturated Cu-N$_4$ sites were the main oxidative species of SACu$_{30}$@NC/PDS system, and the electron shuttle pathway also played a non-negligible role in BPA degradation. Results suggested that Cu(III) and electron shuttle mechanism were caused by the different valence states of copper atoms in Cu-N$_4$ sites. Among them, Cu(I) was more likely to react with adsorbed PDS to form SO$_4^{\bullet-}$ adsorbed on Cu sites (Cu(II)N$_4$-SO$_4^{\bullet-}$) to generate Cu(III), whereas PDS adsorbed on Cu(II) surface was more capable of oxidizing organic micropollutants by extracting electrons from them directly. Owing to the atom distribution and the selective oxidation of nonradicals, SACu$_{30}$@NC exhibited a high metal utilization rate, selectivity for organic pollutants decomposition, and resistance to water matrix interference. Continuous flow experiments proved the good durability of SACu$_{30}$@NC, which further promoted the practical application in the field of wastewater treatment. Overall, this work advanced mechanism understandings of heterogeneous single-atom Cu catalysts associated with persulfate activation and would inspire subsequent research to explore the Fenton-like catalysis in-depth from the atoms valence state of single-atom catalysts.

CRediT authorship contribution statement

Xinyuan Wang: Investigation, Formal analysis. **Jingwen Pan:** Writing – original draft, Investigation, Conceptualization. **Baoyu Gao:** Writing – review & editing. **Lei Wang:** Writing – review & editing, Project administration. **Yue Gao:** Supervision, Resources, Project administration. **Qinyan Yue:** Writing – review & editing, Visualization. **Xing Xu:** Methodology. **Xinyu Yang:** Methodology, Formal analysis. **Congcong Guo:** Investigation, Data curation.

Declaration of Competing Interest

The authors declare that they have no known competing financial interests or personal relationships that could have appeared to influence the work reported in this paper.

Data Availability

Data will be made available on request.

Acknowledgements

Appendix A. Supporting information

Supplementary data associated with this article can be found in the online version at doi:10.1016/j.apcatb.2024.123997.

References

[1] J. Lee, U. von Gunten, J.-H. Kim, Persulfate-based advanced oxidation: critical assessment of opportunities and roadblocks, Environ. Sci. Technol. 54 (2020) 3064–3081.
[2] J. Pan, B. Gao, Y. Gao, P. Duan, K. Guo, M. Akram, X. Xu, Q. Yue, In-situ Cu-doped carbon-supported catalysts applied for high-salinity polycarbonate plant wastewater treatment and a coupling application, Chem. Eng. J. 416 (2021) 129441.
[3] T. Li, J. Pan, X. Wang, Z. Fan, T. Shi, L. Wang, B. Gao, Insights into the fundamental role of Mo doping in facilitating the activation of peroxydisulfate by iron-based catalysts: accelerating the generation of sulfate radicals, Chem. Eng. J. 477 (2023).
[4] C. Yu, C. Yan, J. Gu, Y. Zhang, X. Li, Z. Dang, L. Wang, J. Wan, J. Pan, In-situ Cu-loaded sludge biochar catalysts for oxidative degradation of bisphenol A from high-salinity wastewater, J. Clean. Prod. 427 (2023).
[5] P.G. Tratnyek, J. Hoigne, Oxidation of substituted phenols in the environment a QSAR analysis of rate constants for reaction with singlet oxygen, Environ. Sci. Technol. 25 (1991) 1596–1604.
[6] C. Guan, J. Jiang, S. Pang, C. Luo, J. Ma, Y. Zhou, Y. Yang, Oxidation Kinetics of bromophenols by nonradical activation of peroxydisulfate in the presence of carbon nanotube and formation of brominated polymeric products, Environ. Sci. Technol. 51 (2017) 10718–10728.
[7] K. Qian, H. Chen, W. Li, Z. Ao, Y.N. Wu, X. Guan, Single-atom Fe catalyst outperforms its homogeneous counterpart for activating peroxymonosulfate to achieve effective degradation of organic contaminants, Environ. Sci. Technol. 55 (2021) 7034–7043.
[8] P. Hu, H. Su, Z. Chen, C. Yu, Q. Li, B. Zhou, P.J.J. Alvarez, M. Long, Selective degradation of organic pollutants using an efficient metal-free catalyst derived from carbonized polypyrrole via peroxymonosulfate activation, Environ. Sci. Technol. 51 (2017) 11288–11296.
[9] K. Yin, R. Wu, Y. Shang, D. Chen, Z. Wu, X. Wang, B. Gao, X. Xu, Microenvironment modulation of cobalt single-atom catalysts for boosting both radical oxidation and electron-transfer process in Fenton-like system, Appl. Catal., B 329 (2023).
[10] Z.S. Huang, L. Wang, Y.L. Liu, H.Y. Zhang, X.N. Zhao, Y. Bai, J. Ma, Ferrate self-decomposition in water is also a self-activation process: Role of Fe(V) species and enhancement with Fe(III) in methyl phenyl sulfoxide oxidation by excess ferrate, Water Res 197 (2021) 117094.
[11] B. Liu, W. Guo, W. Jia, H. Wang, Q. Si, Q. Zhao, H. Luo, J. Jiang, N. Ren, Novel nonradical oxidation of sulfonamide antibiotics with Co(II)-Doped g-C3N4-activated peracetic acid: role of high-valent cobalt-oxo species, Environ. Sci. Technol. (2021).
[12] B. Liu, W. Guo, W. Jia, H. Wang, S. Zheng, Q. Si, Q. Zhao, H. Luo, J. Jiang, N. Ren, Insights into the oxidation of organic contaminants by Co(II) activated peracetic acid: the overlooked role of high-valent cobalt-oxo species, Water Res 201 (2021) 117313.
[13] J. Chen, X. Zhou, P. Sun, Y. Zhang, C.H. Huang, Complexation enhances Cu(II)-activated peroxydisulfate: a novel activation mechanism and Cu(III) contribution, Environ. Sci. Technol. 53 (2019) 11774–11782.
[14] Y. Wang, Y. Wu, Y. Yu, T. Pan, D. Li, D. Lambropoulou, X. Yang, Natural polyphenols enhanced the Cu(II)/peroxymonosulfate (PMS) oxidation: the contribution of Cu(III) and HO·, Water Res. 186 (2020) 116326.
[15] W. Hu, Y. Lee, S. Allard, Kinetic and mechanistic investigations of the decomposition of bromamines in the presence of Cu(II), Water Res. 207 (2021) 117791.
[16] L. Wang, H. Xu, N. Jiang, Z. Wang, J. Jiang, T. Zhang, Trace cupric species triggered decomposition of peroxymonosulfate and degradation of organic pollutants: Cu(III) being the primary and selective intermediate oxidant, Environ. Sci. Technol. 54 (2020) 4686–4694.
[17] A. Jawad, K. Zhan, H. Wang, A. Shahzad, Z. Zeng, J. Wang, X. Zhou, H. Ullah, Z. Chen, Z. Chen, Tuning of persulfate activation from a free radical to a nonradical pathway through the incorporation of non-redox magnesium oxide, Environ. Sci. Technol. 54 (2020) 2476–2488.
[18] C. Li, V. Goetz, S. Chiron, Peroxydisulfate activation process on copper oxide: Cu (III) as the predominant selective intermediate oxidant for phenol and waterborne antibiotics removal, J. Environ. Chem. Eng. 9 (2021).
[19] Y. Wei, J. Miao, J. Ge, J. Lang, C. Yu, L. Zhang, P.J.J. Alvarez, M. Long, Ultrahigh peroxymonosulfate utilization efficiency over CuO nanosheets via heterogeneous Cu(III) formation and preferential electron transfer during degradation of phenols, Environ. Sci. Technol. 56 (2022) 8984–8992.
[20] Y. Feng, W. Qing, L. Kong, H. Li, D. Wu, Y. Fan, P.H. Lee, K. Shih, Factors and mechanisms that influence the reactivity of trivalent copper: a novel oxidant for selective degradation of antibiotics, Water Res 149 (2019) 1–8.
[21] F. Li, Z. Lu, T. Li, P. Zhang, C. Hu, Origin of the excellent activity and selectivity of a single-atom copper catalyst with unsaturated Cu-N2 sites via peroxydisulfate activation: Cu(III) as a dominant oxidizing species, Environ. Sci. Technol. 56 (2022) 8765–8775.

[22] C. Xiang, G. Tao, Y. Lifeng, Z. Yuanzheng, N. Junfeng, C.J. C, Exploring the mechanism of electron transfer-mediated peroxymonosulfate activation over Cu-based catalyst for the selective decomposition of bisphenol A, Chem. Eng. J. 471 (2023) 144774.

[23] B. Aristides, K.R. G, K. Pawan, Z. Giorgio, M. Miroslav, T. Jiri, M. Tiziano, T. Ondrej, A. Pavlina, D. Bohuslav, V.R. S, O. Michal, G.M. B, F. Paolo, Z. Radek, Mixed-valence single-atom catalyst derived from functionalized graphene, Adv. Mater. 31 (2019) 1900323.

[24] F. Chen, X.-L. Wu, L. Yang, C. Chen, H. Lin, J. Chen, Efficient degradation and mineralization of antibiotics via heterogeneous activation of peroxymonosulfate by using graphene supported single-atom Cu catalyst, Chem. Eng. J. 394 (2020) 124904.

[25] Q. Wu, J. Wang, Z. Wang, Y. Xu, Z. Xing, X. Zhang, Y. Guan, G. Liao, X. Li, High-loaded single Cu atoms decorated on N-doped graphene for boosting Fenton-like catalysis under neutral pH, J. Mater. Chem. A (2020).

[26] X. Xiao, Y. Gao, L. Zhang, J. Zhang, Q. Zhang, Q. Li, H. Bao, J. Zhou, S. Miao, N. Chen, J. Wang, B. Jiang, C. Tian, H. Fu, A promoted charge separation/transfer system from Cu single atoms and C3 N4 layers for efficient photocatalysis, Adv. Mater. (2020) e2003082.

[27] Y. Gao, Y. Zhu, T. Li, Z. Chen, Q. Jiang, Z. Zhao, X. Liang, C. Hu, Unraveling the high-activity origin of single-atom iron catalysts for organic pollutant oxidation via peroxymonosulfate activation, Environ. Sci. Technol. 55 (2021) 8318–8328.

[28] P. Yang, S. Zuo, F. Zhang, B. Yu, S. Guo, X. Yu, Y. Zhao, J. Zhang, Z. Liu, Carbon nitride-based single-atom Cu catalysts for highly efficient carboxylation of alkynes with atmospheric CO2, Ind. Eng. Chem. Res. 59 (2020) 7327–7335.

[29] T. Zhu, Q. Chen, P. Liao, W. Duan, S. Liang, Z. Yan, C. Feng, Single-atom Cu catalysts for enhanced electrocatalytic nitrate reduction with significant alleviation of nitrite production, Small 16 (2020) e2004526.

[30] S. Wang, W. Wang, L. Yue, S. Cui, H. Wang, C. Wang, S. Chen, Hierarchical Cu2O nanowires covered by silver nanoparticles-doped carbon layer supported on Cu foam for rapid and efficient water disinfection with lower voltage, Chem. Eng. J. 382 (2020) 122855.

[31] L. Kong, G. Fang, Y. Chen, M. Xie, F. Zhu, L. Ma, D. Zhou, J. Zhan, Efficient activation of persulfate decomposition by Cu2FeSnS4 nanomaterial for bisphenol A degradation: kinetics, performance and mechanism studies, Appl. Catal. B 253 (2019) 278–285.

[32] L. Liu, X. Xu, Y. Li, R. Su, Q. Li, W. Zhou, B. Gao, Q. Yue, One-step synthesis of "nuclear-shell" structure iron-carbon nanocomposite as a persulfate activator for bisphenol A degradation, Chem. Eng. J. 382 (2020) 122780.

[33] T. Chen, Z. Zhu, Y. Bao, H. Zhang, Y. Qiu, D. Yin, Promoted peroxymonosulfate activation by electron transport channel construction for rapid Cu(II)/Cu(I) redox couple circulation, Environ. Sci. Nano 8 (2021) 2618–2628.

[34] J. Zhen, S. Zhang, X. Zhuang, S. Ahmad, T. Lee, H. Si, C. Cao, S.-Q. Ni, Sulfate radicals based heterogeneous peroxymonosulfate system catalyzed by CuO-Fe3O4-Biochar nanocomposite for bisphenol A degradation, J. Water Process Eng. 41 (2021).

[35] Y. Sun, J. Yu, X. Zhan, L. Chen, Y. Zhao, H. Wang, H. Shi, A copper-loaded N-doped carbon catalyst with mesoporous hollow sphere structure for bisphenol A removing via peroxymonosulfate activation, Microporous Mesoporous Mater. 342 (2022).

[36] Z. Huang, H. Yu, L. Wang, M. Wang, X. Liu, D. Shen, S. Shen, S. Ren, T. Lin, S. Lei, Ferrocene doped ZIF-8 derived Fe-N-C single atom catalyst to active peroxymonosulfate for removal of bisphenol A, Sep. Purif. Technol. 305 (2023).

[37] Z. Tang, W. Yu, W. Wu, L. Zhu, Y. Ye, C. Gao, B. Wang, S. Ren, Preparation of Fe-Cu bimetal from copper slag by carbothermic reduction–magnetic process for activating persulfate to degrade bisphenol A, J. Taiwan Inst. Chem. Eng. 146 (2023).

[38] W. Ren, L. Xiong, X. Yuan, Z. Yu, H. Zhang, X. Duan, S. Wang, Activation of peroxydisulfate on carbon nanotubes: electron-transfer mechanism, Environ. Sci. Technol. 53 (2019) 14595–14603.

[39] C. Shi, L. Nie, K. Hu, C. Zheng, C. Xu, H. Song, G. Wang, New insights into peroxydisulfate activation by nanostructured and bulky carbons, Appl. Catal., B 325 (2023).

[40] A. Zhang, Y. Zhou, Y. Li, Y. Liu, X. Li, G. Xue, A.C. Miruka, M. Zheng, Y. Liu, Motivation of reactive oxygen and nitrogen species by a novel non-thermal plasma coupled with calcium peroxide system for synergistic removal of sulfamethoxazole in waste activated sludge, Water Res 212 (2022) 118128.

[41] G. Jirui, W. Yujie, S. Yanan, Y. Kexin, L. Qian, G. Baoyu, L. Yanwei, D. Xiaoguang, X. Xing, Fenton- like activity and pathway modulation via single-atom sites and pollutants comediates the electron transfer process, Proc. Natl. Acad. Sci. 121 (2023) e2313387121.

[42] Y. Ding, L. Fu, X. Peng, M. Lei, C. Wang, J. Jiang, Copper catalysts for radical and nonradical persulfate based advanced oxidation processes: certainties and uncertainties, Chem. Eng. J. 427 (2022).

[43] S. Sun, C. Shan, Z. Yang, S. Wang, B. Pan, Self-enhanced selective oxidation of phosphonate into phosphate by Cu(II)/H2O2: performance, mechanism, and validation, Environ. Sci. Technol. 56 (2022) 634–641.

[44] S. Sun, J. Jiang, L. Qiu, S. Pang, J. Li, C. Liu, L. Wang, M. Xue, J. Ma, Activation of ferrate by carbon nanotube for enhanced degradation of bromophenols: kinetics, products, and involvement of Fe(V)/Fe(IV), Water Res 156 (2019) 1–8.

[45] K.Z. Huang, H. Zhang, Direct electron-transfer-based peroxymonosulfate activation by iron-doped manganese oxide (delta-MnO2) and the development of galvanic oxidation processes (GOPs), Environ. Sci. Technol. 53 (2019) 12610–12620.

[46] W. Ren, L. Xiong, G. Nie, H. Zhang, X. Duan, S. Wang, Insights into the electron-transfer regime of peroxydisulfate activation on carbon nanotubes: the role of oxygen functional groups, Environ. Sci. Technol. 54 (2020) 1267–1275.

[47] P. Shao, Y. Jing, X. Duan, H. Lin, L. Yang, W. Ren, F. Deng, B. Li, X. Luo, S. Wang, Revisiting the graphitized nanodiamond-mediated activation of peroxymonosulfate: singlet oxygenation versus electron transfer, Environ. Sci. Technol. 55 (2021) 16078–16087.

[48] T. Zhang, Y. Chen, Y. Wang, J. Le Roux, Y. Yang, J.P. Croue, Efficient peroxydisulfate activation process not relying on sulfate radical generation for water pollutant degradation, Environ. Sci. Technol. 48 (2014) 5868–5875.

[49] Z. Xiaoyan, Z. Shan, Y. Yong, W. Liguang, M. Zijie, Z. Haishuang, Z. Xiaoqing, X. Huanhuan, X. Hongyin, H. Bolong, L. Jing, G. Shaojun, W. Erkang, A general method for transition metal single atoms anchored on honeycomb-like nitrogen-doped carbon nanosheets, Adv. Mater. 32 (2020) 1906905.

[50] W. Guobin, L.D. Un, R. Bohua, H.F. M, J. Gaopeng, C.Z. P, G. Jeff, C. Eric, B. Zhengyu, Y. Lin, C. Zhongwei, Orbital interactions in Bi-Sn bimetallic electrocatalysts for highly selective electrochemical CO2 reduction toward formate production, Adv. Energy Mater. 8 (2018) 1802427.

[51] T. Fan, X. Yao, Z. Sun, D. Sang, L. Liu, H. Deng, Y. Zhang, Properties and metal binding behaviors of sediment dissolved organic matter (SDOM) in lakes with different trophic states along the Yangtze River Basin: a comparison and summary, Water Res 231 (2023) 119605.

[52] S. Yao, N. Ni, X. Li, N. Wang, Y. Bian, X. Jiang, Y. Song, N.S. Bolan, Q. Zhang, D.C. W. Tsang, Interactions between white and black carbon in water: a case study of concurrent aging of microplastics and biochar, Water Res 238 (2023) 120006.